Two regimes of the equatorial warm pool.

Part II: Hybrid coupled GCM experiments

Masahiro Watanabe[1]

Faculty of Environmental Earth Science, Hokkaido University

Journal of Climate

Submitted on July 19, 2007

Revised on December 6, 2007

Corresponding author:

M. Watanabe, Faculty of Environmental Earth Science, Hokkaido University

N10W5 10, Sapporo, Hokkaido 060-0810, Japan

E-mail: hiro@ees.hokudai.ac.jp

---

[1] Present affiliation: Center for Climate System Research, University of Tokyo. 5-1-5 Kashiwanoha, Kashiwa, Chiba, Japan

ABSTRACT

In this Part II, two regimes in a simple tropical climate model identified in Part I are verified using a hybrid coupled general circulation model (HCM) that can reproduce observed climatology and the interannual variability reasonably well. Defining a ratio in basin width between the Pacific and Indian Oceans, a series of parameter sweep experiments was conducted with idealized tropical land geometry. Consistent with the simple model, the HCM simulates two distinct states: the split warm pool regime with large vacillation between the two ocean basins and the single warm pool regime representing current climate, the former being suddenly switched to the latter as the Pacific becomes wider than the Indian Ocean. Furthermore, the vacillation in the split regime reveals a preferred transition route that the warm phase in the Pacific follows that in the Indian Ocean, occurring due to convectively coupled Kelvin waves which accompany precipitation anomalies over land. Additional experiments show that inclusion of the idealized Eurasian continent stabilizes the split regime by reducing the Bjerknes feedback in the Indian Ocean, suggesting the atmosphere-ocean-land interaction at work in maintaining the observed warm pool. Difference in cloud feedback was not found between two regimes, which may be model-dependent though.

Both of the simple model and the HCM results suggest that the tropical atmosphere-ocean system inherently involves multiple solutions, which may have an implication to the climate modeling as well as to understand the observed mean climate.

1. Introduction

The climatological mean state in the tropics has a well organized structure which consists of the Hadley and Walker circulations in the atmosphere and a set of warm pool and cold tongue in the ocean. In particular, the equatorial warm pool widely spread around the maritime continent, over which the latent heat release due to deep convections is prominent, is regarded as driver for the large-scale atmospheric circulation.

A number of mechanisms have been proposed for generating and maintaining the warm pool sea surface temperature (SST) which is relatively uniform around 28°C (Li et al. 2000; Clement et al. 2005). Some are the atmospheric processes such as the cirrus cloud thermostat (Ramanathan and Collins 1991), surface evaporation feedback (Hartmann and Michelesen 1993) and radiative forcing associated with the tropospheric humidity (Pierrehumbert 1995), but others are the oceanic (Sun and Liu 1996; Clement et al. 1996). They primarily explain the spatial homogeneity of the warm pool SST, but presence of the warm pool can be attributed to coupled atmosphere-ocean processes, often called the climatological Bjerknes feedback (Bjerknes 1969; Neelin and Dijkstra 1995). For example, active convections over the warm pool induce the surface easterly and westerly winds over the equatorial Pacific and Indian Oceans, respectively, which in turn force the thermocline tilt that accompanies the warm thick surface water piled up to the Indonesian region. This climatological feedback at the same time gives rise to the upwelling in the eastern equatorial Pacific, where the cold tongue is developed, while suppresses such an oceanic cooling in the eastern Indian Ocean because of the westerly stress.

Several studies have shown that the Bjerknes feedback is commonly operating to

maintain the climatological state and to generate the El Niño-Southern Oscillation (ENSO) phenomenon (e.g., Jin 1996). Dijkstra and Neelin (1995) demonstrated that the warm pool-cold tongue contrast observed in the Pacific is sensitive to parameter changes that control the climatological Bjerknes feedback even though the background easterly associated with the Hadley circulation always tends to generate zonal gradients in SST and thermocline depth. Furthermore, the warm pool around the maritime continent should affect the surface wind stresses both over the Pacific and the Indian Ocean, so that the warm pool may be understood as a product of the coupled system in these ocean basins as a whole. Therefore, we would like to address a question from a wider point of view of what the critical condition is for the single warm pool realized between the Indian Ocean and the Pacific as observed.

In a companion paper of Watanabe (2007, hereafter referred to as Part I), a simple tropical model was used to illustrate that the coupling of two oceans is crucial for generating the single, wide spread warm pool around the maritime continent. Furthermore, the simple model suggests that such a climatological state, called *single warm pool regime*, is not a unique solution of the tropical coupled system; another branch of solution emerges if the Indian Ocean is wider than observed. This state called the *split regime*, which accompanies warm pools separated into the western basin of each ocean, is not stable hence exhibits a large amplitude vacillation between two oceans that looks like “super El Niño”. Since the model used in Part I is highly truncated, the above results must be verified with a higher order realistic model of the tropical climate. For this purpose, we use a hybrid coupled model (HCM) to conduct a series of numerical experiments with varying a control parameter same as in Part I.

This paper is organized as follows. In the next section, the HCM used in this Part II is described. Results of a reference experiment using the realistic boundary conditions are presented in section 3 in order to validate the ability of the HCM. In section 4, a series of the idealized HCM experiments is performed. The overall results support the existence of two regimes in the tropical climate as found in the simple model. We further present in section 4 details of the vacillation cycle occurred in the split regime and sensitivity of the climatological states to other factors such as the Asian sub-continent and the Atlantic Ocean. Section 5 gives discussion, followed by conclusions of the two-part papers in section 6.

2. Hybrid coupled model

The HCM used in this study consists of the atmospheric general circulation model (AGCM) coupled to a simpler 2.5-layer ocean model. While a hybrid model based on the ocean GCM coupled to a simple atmospheric model has sometimes been constructed for ENSO studies (e.g. Neelin 1990), we employ the expensive model for the atmosphere since, as argued in the introduction of Part I, warm pool physics includes complicated atmospheric processes such as precipitation, cloud and radiation. A similar approach is taken, for example, for investigating the intraseasonal variability in the tropical atmosphere affected by ENSO (Fu et al. 2007).

The AGCM used is the atmospheric component of a global climate model called MIROC (K-1 model developers 2004), which is one of the Japanese community models collaboratively developed at the Center for Climate System Research (CCSR), the University of Tokyo, the National Institute for Environmental Studies (NIES), and the Frontier Research Center for Global Change (FRCGC). MIROC has been contributing

to the IPCC AR4 (e.g., Lin et al. 2005) and is widely used to study past, present and future climate changes (Emori et al. 2004; Kimoto 2005; Nozawa et al. 2005, among others). The atmospheric component model, referred to as the CCSR/NIES/FRCGC AGCM, contains a standard physics package such as the cumulus convection, cloud, turbulence closure and radiation schemes. We use a course horizontal resolution of T42 and vertical 20 layers on σ-surfaces in which 5 layers reside in $\sigma \geq 0.8$.

The ocean model is derived from the 2.5-layer shallow-water model developed by McCreary and Lu (1994). The model solves fully nonlinear equations of motion incorporated with the thermodynamics for the upper and lower layers above the deep ocean where we assume no motion with constant temperature. The mixed layer parameterization is based on a simple bulk turbulence model in which the entrainment velocity is represented in terms of the upper layer thickness adjusted towards a reference value of 50 m with the timescale of 1 day (Eq. (5) of McCreary and Lu 1994). The horizontal resolution is 1°×0.5° for resolving the equatorial waves. We use the no-slip boundary condition and assume no diffusion of heat and mass across the boundary. When either the northern or southern boundary of the model domain is not the same as the basin boundary, the upper layer temperature at the nearest 2.5° to the model boundary is restored to the observed monthly SST climatology with the timescale of 10 days. The model equations include harmonic and bi-harmonic eddy viscosity terms for momentum as well as the harmonic diffusion for temperature with the coefficients of 1×10^4 m^2 s^{-1}, 2×10^{13} m^4 s^{-1} and 5×10^3 m^2 s^{-1}, respectively. Other constants follow McCreary and Lu (1994).

After the AGCM and the shallow-water ocean model are spun up separately, the HCM is constructed by coupling them in the region of interest. The two media exchange

heat and momentum once a day. The detail for the ocean model domain and the spin-up procedures will be described in the subsequent sections. Note that we have not applied any flux correction.

3. Control experiment

Preceding the HCM experiments with idealized boundary conditions, we examined the extent to which the HCM can reproduce observed climatology and the interannual variability. Using the realistic orography, the atmospheric component model driven by the observed SST climatology (Rayner et al. 2003) was spun up for 3 years whereas the ocean model which covers the entire Pacific and Indian Oceans (40°S-60°N) was spun up for 30 years under the observed wind stress forcing (Hellerman and Rosenstein 1983) and the restoring to observed SST climatology with the relaxation time of 10 days. After coupling these models, the HCM was integrated for 110 years, referred to as the control run, in which the SST outside of the ocean model is prescribed to the monthly observed climatology.

In Fig. 1 we compare the annual mean climatology and the interannual variability in the control run with those observed. The HCM is shown to reproduce the wide-spread warm pool between the Indian Ocean and the western Pacific reasonably well albeit the maximum SST is slightly lower than observations (Figs. 1a and 1d). There is also a discrepancy that the equatorial Pacific is much cooler in the model probably due to simplified representation of the upwelling. These cooling biases are reflected in the precipitation climatology as well (Figs. 1b and 1e). The total precipitation is slightly less than the observations besides the intense precipitation observed to the east of Indonesia has not been reproduced in the HCM. Nevertheless,

the model precipitation pattern is similar in many respects to the observed distribution such as the single ITCZ. Given the fact that some of more sophisticated CGCMs still suffer from a bias toward the double ITCZ (Covey et al. 2003), reality of the climatological SST and precipitation shown by the HCM appears to be sufficient for the purpose of this study.

Furthermore, the HCM control run produces the ENSO-like interannual variability. The pattern of the monthly SST standard deviation is roughly close to the observation, which represents maxima in the equatorial Pacific and the North Pacific both associated with ENSO (Figs. 1c and 1f). While the amplitude of ENSO as measured by the standard deviation of the Niño 3 SST time series in the control run is about two third of the observed value, the SST and sea level pressure (SLP) anomalies regressed upon the Niño 3 SST anomaly reveal that the HCM can reproduce signature of ENSO and associated atmospheric bridge over the North Pacific (not shown). This result further encourages us to use the HCM with idealized experimental design.

4. Parameter sweep experiments with idealized land geometry

Provided that the HCM reproduced observed climate to a certain degree, we perform a series of the idealized HCM experiments in which the ocean model covers the entire tropics between 43.5°S-43.5°N separated by three rectangle continents having the equal longitudinal extent of 30° with flat topography of 10 m (Fig. 2a). At latitudes poleward of the ocean model boundary, zonally averaged, observed SST climatology is given to the AGCM. In order to verify the results in Part I, the control parameter α is defined in a similar manner:

$$\alpha = \frac{L_2}{L_1} - 1 \qquad ,$$

where L_1 and L_2 denote the length for the left-hand-side and the central ocean basins in Fig. 2, respectively. The highly idealized land-ocean geometry is regarded as a prototype of the real world, so that these two ocean basins are simply referred to as the "Indian Ocean" and the "Pacific Ocean" (double quotations dropped for convenience in the rest of this paper). The basin length for the idealized Atlantic Ocean is fixed at 60° and therefore $L_1 + L_2$ is also constant of 210°. The role of the Atlantic Ocean is discussed in section 4d; elsewhere we focus on the Indo-Pacific region.

For different values of α, the HCM is integrated for 50 years with the seasonal cycle in solar insolation, in which the last 45 years are used to make the climatological state. We start the experiment with α=0 (denoted as A0) and the last state is used as initial conditions for the next experiment with α=0.2 (A2). By repeating this procedure we carry out the experiments A0, A2,…, A14. As in Part I, the two ocean basins have equal length in A0 whereas the Pacific is twice as wide as the Indian Ocean in A10. To investigate the dependence of the climatological state on initial conditions, another series of experiments is performed in a similar manner to the A-runs but from α=1.4 to α=0.4, referred to as B14, B12, …, B4, which will be described in section 4b.

a. Two regimes in the HCM

Figure 2 shows the annual mean climatology in A0, which reveals a fundamental picture of tropical climate. Namely, the warmest SST is found in the western side of each ocean, collocated with the tilted equatorial thermocline (Fig. 2a). Since the land geometry is symmetric about the equator, off-equatorial cold tongue is not well

produced in the eastern basin hence the double ITCZ is prevailing (Fig. 2b). The western boundary currents associated with the subtropical gyre transport heat, resulting in an enhancement of the subtropical evaporation at the western edge of the ocean (Fig. 2c). As expected, the climatological mean states are nearly identical in the Indian Ocean and the Pacific.

Simple model has predicted that the mean state as shown in Fig. 2 is not stable (cf. section 3 of Part I). Indeed, the time-longitude section of the equatorial SST indicates that an irregular vacillation occurs between the two oceans (Fig. 3a). For example, during years 10-15 the Indian Ocean is occupied by the uniform SST of more than 26°C, which is akin to El Niño but with much larger magnitude and longer duration. Such an El Niño-like state in the Indian Ocean is switched to the normal or La Niña-like state in the subsequent years, when the Pacific experiences the El Niño-like warm state. In the experiment A14, there is no such a large amplitude vacillation and a single warm pool is stably maintained between the Indian Ocean and the Pacific (Fig. 3b). This result is quite consistent with the finding in the simple model analysis of Part I which has identified the split warm pool regime and the single warm pool regime although the vacillation period in the HCM is doubled to that in the simple model. The regime transition in the HCM will be examined in the next subsection.

It appears that in A0 the Pacific warm state tends to follow that in the Indian Ocean. This is highlighted in the trajectory plot of the so-called cold tongue SST in the two ocean basins (Fig. 4), where the cold tongue is defined by the rectangular area of 4°S-4°N and the eastern half of the basin, the length varying with α. Scatter plot of the monthly mean values are somewhat noisy (small dots in Fig. 4), but the trajectory of the low-frequency components (circles in Fig. 4) clearly indicates the preferred transition

route from the Indian Ocean to the Pacific in A0 (Fig. 4a). In A14, cold tongue SSTs are simply negatively correlated, the variability larger in the eastern Pacific (Fig. 4b) in association with the idealized version of ENSO as simulated in the control run.

The vacillation behavior found in A0 is further examined by means of the lagged composite of monthly anomalies, i.e., deviation from monthly climatology, with reference to the cold tongue SST time series in the Pacific. Based on the time when the cold tongue SST shows the highest value, the composite anomaly fields are calculated from -7 to +7 years. Shown in Fig. 5 are the lagged composite anomalies in SST, thermocline depth and precipitation along the equator in A0. The SST anomalies again exhibit the transition of warm states from the Indian Ocean to the Pacific, taking about 4 years (Fig. 5a). Besides, the warm state in the Pacific is followed by the warming of the Atlantic Ocean. The composite SST anomalies with reference to the cold tongue SST in the other oceans result in a similar result, which indicates that the eastward propagation of positive SST anomalies are circumglobal (not shown). In each ocean basin, the surface warming accompanies the shoaling (deepening) of the thermocline in the western (eastern) part, which is due to the weakened surface easterly (Fig. 5b). The westerly wind stress anomaly seems to be driven by the anomalous positive precipitation over the entire equatorial ocean (Fig. 5c). These anomalies are quite consistent with the signature of the Bjerknes feedback, which can explain why the warming occurs in one ocean basin but cannot explain why the warming in a basin follows that in the adjacent western basin. Simple model in Part I tells us the divergence over the continent leading to the transition, which may be identified around 120°E at years -2 to 0 but not quite evident (Fig. 5c).

To obtain further insights into the mechanisms of the preferred eastward

migration of the warm state, the composite maps at lags -4, -2, 0 and 2 years are presented in Fig. 6. At lag -4 years, the warm state appears in the Indian Ocean, which accompanies a weak cold state in the Pacific (Fig. 6a). The thermocline is tilted at this time such that the warm pool becomes deep in both sides of the continent around 120°-150°E, which is also associated with the anomalous westerly and easterly over the equatorial Indian Ocean and the Pacific, respectively (Fig. 6e). These stress anomalies result in the thermocline uniformly shoaled (deepened) in the Indian Ocean (Pacific) two years later by exporting (importing) the surface water poleward (equatorward) (Fig. 6b). The deepened thermocline in the eastern Pacific suppresses the surface cooling due to upwelling hence the El Niño-like warm state develops at year 0 (Fig. 6c). Except for the extremely large amplitude of the anomaly (the maximum SST anomaly greater than 5 K!), overall time evolution, including the duration of the cycle, of the composite SST, thermocline and surface wind anomalies in the respective ocean is reminiscent of that of El Niño. The cold tongue SST and the zonally averaged equatorial thermocline depth are oscillating in quadrature (not shown), which is well suited for the recharge oscillator concept (Jin 1997).

On one hand, the transition from warm to cold states and vice versa is nearly out of phase between the Indian Ocean and the Pacific. On the other hand, the warm state occurred at year -4 (year 0) in the equatorial Indian Ocean (Pacific) is much stronger than the concurrent cold state. The relative magnitude between the warm and cold states is opposite to the vacillation cycle in the conceptual model (Fig. 4b of Part I). In the idealized HCM experiments, the climatological mean state is slightly cool (Fig. 2a), so that the SST anomaly is not limited by the radiative-convective equilibrium during the warm state unlike the solution in the conceptual model.

The processes responsible for the eastward migration can be identified between lags -4 and 0 years, from one El Niño-like state in the Indian Ocean to another in the Pacific. At lag -4 years, the maximum precipitation anomaly is found near the western edge of the continent around 120°E, plausibly induced by the convergence associated with the westerly anomaly over the Indian Ocean (Fig. 6e). Indeed, the upper level divergence anomaly has the center aloft (not shown). Since the convectively coupled Kelvin waves are enhanced when the source is placed to the west of the basic state warm SST (cf. Watanabe and Jin 2003, their appendix), the anomalous easterly in the western Pacific appears to be intensified by the positive precipitation anomaly around 120°E. The westward stress anomaly then forces oceanic Rossby and Kelvin responses (Fig. 6a), which triggers the developing El Niño-like state in the Pacific Ocean during the subsequent 4 years. The crucial role of convections over land to the west of ocean for ENSO has been pointed out by Anderson and McCreary (1985a). The results of the composite analysis in our experiments are quite consistent with their finding, indicating that the anomalous convection over the "maritime continent" between 120°-150°E is actively working to the eastward propagation of the El Niño-like signals. This is also consistent with the assumption made in Part I in which the surface wind convergence over land which implicitly represents the convection there couples the atmosphere-ocean system in the adjacent two ocean basins.

b. Dependence on α

The equatorial SST and other fields simulated in A0 and A14 are conceivably corresponding to the split warm pool and the single warm pool regimes called in Part I. It will therefore be intriguing to examine the regime transition with respect to change in

α. For each run employing different α from 0 to 1.4 (A0-A14), we defined the cold tongue SST in the Pacific and then plotted the annual mean climatology as a function of α (dots in Fig. 7).

As far as the climatological mean values are concerned, the cold tongue is weaker for smaller α and smoothly strengthens as α increases. However, the time evolution of the equatorial SST in A0 (cf. Fig. 3a) indicates that the climatological mean state does not make sense in the vacillating regime, which is confirmed by the standard deviation of the cold tongue SST much larger for $\alpha \le 0.8$ (error bars in Fig. 7). Therefore, maxima in probability distribution of the monthly cold tongue SST, instead of the climatological mean values, are calculated to identify the regime transition (triangles in Fig. 7). It clearly measures the split regime at $\alpha \le 0.8$ where two maxima, one below 22°C and another about 28°C, are present. For $\alpha \ge 1$, the single maximum of the probability distribution matches the climatological mean SST. In the simple tropical model presented in Part I the transition has occurred around α=0.7, which is not far from the threshold identified in the HCM. In the HCM experiments α is crudely descretized, but Fig. 7 strongly suggests that the transition between two regimes can occur in a narrow range of α, when the Pacific is roughly twice as wide as the Indian Ocean.

It should be noted that the spatial patterns associated with the vacillation cycle for $0.2 \le \alpha \le 0.8$ are similar to those presented in Figs. 5 and 6, but the interval is lengthened besides the amplitude becomes larger (smaller) in the Pacific (Indian Ocean) for larger α. These changes have all been obtained with the simple model as well.

The annual-mean cold tongue SST in the B-runs was also examined (results not shown). The climatological mean values in the Pacific remain around 20 °C between

α =0.4 and α =1.4, indicating that the single regime continues to be present in those runs. While this suggests that the HCM exhibits multiple regimes as in the conceptual model, longer time integration may be necessary to obtain more robust results.

c. Role of the Asian sub-continent

In A14, and likewise in A10 and A12, the single warm pool does emerge around the maritime continent. However, the zonal extent is short because the warm SST to the west of the maritime continent is not sufficiently generated compared to the observation and the control run (Fig. 3b). We have so idealized the land geometry that several mechanisms may work to differentiate the idealized HCM climatology from the observations. In order to identify the leading mechanism among them, the climatological states are compared between the HCM and the observation.

Figure 8a shows the annual mean climatology of SLP and the vertical pressure velocity at 500 hPa (denoted as ω_{500}) derived from the NCEP-NCAR reanalysis (Kalnay et al. 1996). The ω_{500} field indicates a broad region of ascent over the eastern Indian Ocean and the western Pacific, which well coincides with the extent of the warm pool. Over the extratropics between 60°-120°E, a high SLP center which is a part of the subtropical high is found in both hemispheres, resulting from the steady Rossby response to the diabatic heating over the warm pool region as measured by positive ω_{500} to the east of the SLP centers.

A similar climatological state of the atmosphere is produced in A10 (Fig. 8b). The equatorial ascent is concentrated over land but not found over the eastern Indian Ocean, which is due to cooler SST. The anticyclonic surface winds associated with the subtropical high not only drive the subtropical gyres but also force the zonal tilt in

equatorial thermocline (Fig. 8c). In the eastern equatorial Indian Ocean, the thermocline becomes shallow due to this wind stress forcing, which initiates the Bjerknes feedback and thereby favors cooler SST counteracting the convergence feedback associated with the Pacific side of the warm pool. A fundamental difference between nature and the idealized HCM is the presence of the Asian sub-continent which prohibits the Bjerknes feedback over the northern part of the ocean. Therefore we conducted an additional experiment similar to A10 except for an idealized Eurasian continent included to the north of 20°N, referred to as the E10 run.

The impact of the added Eurasian continent is the most striking during boreal summer when the monsoon circulation is established. In E10, the surface cross-equatorial flow akin to observations is produced during summer (Fig. 9b), which has not found in A10 (Fig. 9a). The ITCZ over the tropical Indian Ocean is also shifted northward in E10 due to convergence over the Asian sub-continent. As argued above, the Bjerknes feedback in E10 is prohibited by the continent in the northern Indian Ocean, leading to the warming (cooling) in the eastern (western) equatorial Indian Ocean as identified by the difference in annual mean SST between E10 and A10 (Fig. 9c). The reduced Bjerknes feedback due to presence of the idealized Eurasian continent may thus explain qualitatively why the warm pool is weak in the Indian Ocean side in A10. However, the warming effect for the eastern Indian Ocean is at most 1 K in Fig. 9c, which may not be sufficient in magnitude. Since the HCM control run shows the warm pool spread enough in the Indian Ocean (Fig. 1d), this failure may be attributed to the idealized land configuration.

In Fig. 10 we compared the surface zonal wind over the equatorial Indian Ocean among E10, control run and the NCEP-NCAR reanalysis. The zero contour of the zonal

wind in A10 is superimposed in Fig. 10a, which indicates that the equatorial westerly in E10 extends westward during spring and autumn but reduced during summer. The stronger equatorial easterly in summer works to cool the central and eastern Indian Ocean via the upwelling, which would counteract the reduced Bjerknes feedback settled by the presence of the Asian sub-continent in E10. In reality, both the control run and the reanalysis data do not reveal the prevailing easterly during summer; the equatorial westerly exists in the western half of the Indian Ocean (Figs. 10b and 10c). The horizontal circulation maps clearly exhibit that this surface westerly is associated with the monsoon southwesterly redirected towards southeast by the protruded Indian sub-continent (not shown). It is therefore plausible that the specific shape of the actual Asian sub-continent which distorts the summer monsoon circulation hence regulates the equatorial upwelling is important for sufficiently warming the eastern Indian Ocean.

Despite the weak influence to the climatological mean SST, the inclusion of the Asian sub-continent is crucial in terms of the regime behavior. We further performed the experiments E2-E10 similar to the E0 run but with varying α. The results are not shown, but the regime diagram for these runs reveals that the split regime disappeared. This is again interpreted as the continental effect in reducing the climatological Bjerknes feedback. The Bjerknes feedback in the Indian Ocean would be roughly half compared to that in the Pacific even with $\alpha = 0$, so that the Pacific Ocean can drive the climatological states in the whole tropics, which is qualitatively similar to the situation observed in the single warm pool regime. This indicates that the regimes are fundamentally dependent upon the relative strength in Bjerknes feedback between the two oceans and there will be parameters alternative to α for the presence of two regimes.

d. Interaction with the Atlantic Ocean

The results presented previously indicate that the HCM behaves in a similar manner to the simple model used in Part I despite the large difference in their degrees of freedom. In reality, the HCM is much more complex than the simple model, so that we need to examine carefully whether the elements governing the two regimes in the HCM are the same as those in the four-order model of Part I.

A possible concern is the extent to which the regimes are affected by the active Atlantic Ocean in the HCM. Figure 11a displays the annual mean climatology of the equatorial SST in the Atlantic, which reveals that the zonal SST distribution is distinct between the two regimes. For the single warm pool regime of $\alpha \geq 1$, the SST is warm (cold) in the western (eastern) Atlantic similar to the observations whereas for the split regime of $\alpha \leq 0.8$ a wide area of the central equatorial Atlantic is occupied by SST lower than 24.5 °C, which is induced by the strong upwelling. The amplitude of the SST variability is also quite different between the regimes; the Atlantic SST in the split regime shows much larger interannual variability than that in the single warm pool regime (Fig. 11b). The two regimes are thus identified clearly in the Atlantic Ocean as well as in the other oceans. Indeed, the eastward propagation of SST anomalies in the split regime is continuous along all the ocean basins (cf. Fig. 5a), indicating that the Atlantic is also a part of the vacillating regime.

To isolate the role of the interactive Atlantic Ocean, an additional experiment was performed with $\alpha = 0$ but the Atlantic SST prescribed to the monthly climatology obtained from A0, referred to as the AP0 run. The equatorial SST in AP0 is then compared to that in A0 (Fig. 12). It is evident that the time evolution of the equatorial SST is qualitatively similar to each other even though the vacillation is less frequent in

AP0. By referring to the eastward propagation embedded in the vacillation cycle (see section 4a), it may be natural that AP0 which lacks the triggering for warm states in the Indian Ocean exhibits less frequent occurrence of the vacillation. We confirmed that the vacillating split regime is still present even when the Atlantic SST is prescribed to the monthly climatology obtained from A10 (results not shown). To summarize, the active Atlantic Ocean affects the other ocean basins to some extent but the influence is not crucial as far as the Atlantic basin length is fixed to be narrow, leading to the conclusion that the regime behavior can essentially occur in the coupled Indo-Pacific climate.

e. Cloud-radiative feedback

As mentioned in the introduction, previous studies have advocated the dominant role of atmospheric processes, in particular cloud feedback, for regulating the warm pool SST. It is therefore worth examining the difference in cloud-radiative forcing between the two regimes in the HCM. The annual mean climatology of the total cloud cover in A0 and A14 is shown in Fig. 13. Since most of AGCMs are not capable of reproducing the subtropical low clouds besides the off-equatorial cold tongues are not well generated in the series of the idealized HCM experiments, the cloud cover largely reflects the upper level anvil associated with the deep convection.

The cloud cover over the equatorial strip in A14 is roughly 10 % more than that in A0, which will be reasonable from the associated convective precipitation (not shown) that is intense in the single warm pool regime. If the shortwave cooling associated with the upper-level anvil dominates its greenhouse effect, the increased cloud cover in A14 will act to suppress the single warm pool via the increased radiative cooling. To see the change in cloud effect between the two regimes, the cloud radiative

forcing along the equator is plotted for A0 and A14 (Fig. 14). The cloud shortwave forcing is relatively uniform, roughly -60 W m^{-2} along the equator. While the difference is not quite clear, the shortwave cooling averaged over lands is slightly stronger in A14 than in A0, the former -54.7 W m^{-2} and the latter -51.5 W m^{-2}. Similarly the cloud longwave forcing is positive everywhere, but the land-sea contrast is larger than the shortwave forcing. It is noted that the longwave warming is also stronger in A14, showing the land average of 64.1 W m^{-2} compared to 58.9 W m^{-2} in A0. This results in the net cloud radiative forcing in the two runs is similar in magnitude to each other, indicating that the change in cloud cover does not affect significantly the difference in climatological state between the two regimes. We should, however, keep it in mind that the magnitude and even sign of the cloud radiative forcing may depend on the parameterization employed in the model.

5. Discussion

The two regimes of the tropical climate is not the first depicted in the present study. In an extension of Anderson and McCreally (1985a) who simulated the El Niño-like oscillation in a simple coupled model, Anderson and McCreally (1985b) coupled two oceans to a linear atmospheric model. They have obtained three solutions for the basin configuration with equal length, larger “Pacific” and larger “Indian Ocean”: two oceans are oscillating, the “Indian Ocean” is stable but the “Pacific” oscillates, both oceans are stable, respectively. Except for the last case, the Anderson and McCreally’s solutions are surprisingly similar to the split and the single warm pool regimes identified in the present HCM. We conducted the numerical experiments in a systematic manner using the GCM-based coupled model, so that our results may be somewhat

beyond their pioneering work. The conclusions are also slightly different depending upon the focus of the study; Anderson and McCreally concluded that the narrow Indian Ocean having a stable warm pool in its east is setting the necessary condition for the Pacific El Niño whereas we conclude that the Bjerknes feedback in the Indian Ocean much weaker than the Pacific one, achieved by the narrow basin length or by alternative factors (cf. section 4c), is the necessary condition of the observed warm pool *per se*.

Both in Parts I and II, we have defined the control parameter of the relative basin length between the Indian Ocean and the Pacific but not their absolute lengths. If we use the latter as a primary parameter, a richer regime behavior may be obtained since the total basin length becomes another free parameter. In short, for the total length much shorter than 210° used in the present experiments, the coupled Pacific-Indian Ocean would settle in the split regime even with $\alpha > 0.8$ because of the interaction with the wide Atlantic Ocean. There may also be another regime of the simple radiative-convective equilibrium where the Bjerknes feedback is not sufficient to create the warm pool-cold tongue contrast both in the Indian Ocean and the Pacific. This is indeed happening in the simple model (not shown), but in the HCM which has the finite Earth surface the lengthened Atlantic Ocean will dominate the regime in which the single warm pool may occur between the Pacific and the Atlantic. One exception may be the experiment in which the Earth radius is changed; on a smaller planet akin to Earth the purely radiative-convective equilibrium may be achieved with any of the tropical land configuration. These arguments indicate that the narrow Atlantic Ocean is the necessary condition for the presence of the observed warm pool around the maritime continent.

Results in section 4c highlighted that the Indian Ocean can be stabilized by narrowing the length or by introducing the Asian sub-continent both of which reduce

the climatological Bjerknes feedback there hence act to create the single warm pool. In observations, the summer monsoon flow that is redirected by the Indian sub-continent accompanies the equatorial westerly in the western Indian Ocean, which may also have a similar effect. Since the idealized experiments have not shown such an effect, a realistic coupled model simulation like the control run but without the Indian sub-continent will provide useful insights into that question. While the coupling between ENSO and the Asian summer monsoon variability has been extensively investigated in literature, the role of the atmosphere-ocean-land interaction in mean climate in association with the monsoon circulation, Indian Ocean dynamical processes and the warm pool is not fully elucidated, which should be done for better climate modeling.

The coupled Indo-Pacific system may also be affected by other factors. While the oceans are strongly coupled via the atmospheric circulation as has been assumed in the present work, the oceanic connection via the Indonesian throughflow can impact the mean state as well as the variability in the Indo-Pacific climate (Schneider 1998; Song et al. 2007, among others). The Indonesian throughflow transports warm surface water from the western Pacific to the eastern Indian Ocean where the Sverdrup circulation is also weakened by the throughflow. They act to warm the Indian Ocean side of the warm pool hence would maintain the single warm pool regime. A recent coupled GCM study by Song et al. (2007) suggests approximately 1 K difference in SST of the eastern Indian Ocean by opening/closing the passage of the Indonesian throughflow, which is as effective as the presence of the Asian sub-continent (our Fig. 9).

6. Conclusions

In the two-part papers, we examined the fundamental behavior of the tropical

climate system as represented by the simple coupled model and the HCM in order to help understanding current mean climate, in particular the presence of the warm pool. By choosing the relative basin width of the Indian Ocean and the Pacific as a control parameter, we explored the model solutions dependent upon it and found that:

- The tropical climate has two regimes depending upon the relative basin width: one with the single warm pool around the maritime continent as observed and another with the warm pools split into the western part of each ocean basin.
- The split warm pool regime which appears when the Indian Ocean is as wide as the Pacific is switched to the single warm pool regime in a narrow range of the parameter, the transition occurring for the Pacific roughly twice as wide as the Indian Ocean.
- The split warm pool regime is not stable, so that the coupled oscillation takes place between the two oceans, each of which is fluctuating similar to ENSO but with much larger amplitude. There is a preferred eastward propagation of the El Niño-like warm state, which is likely to result from the convectively coupled Kelvin wave response in the atmosphere that can influence the surface wind over the adjacent eastern ocean.
- Asian sub-continent prohibits the climatological Bjerknes feedback in the northern Indian Ocean hence stabilizes the split warm pool regime by warming the eastern Indian Ocean.

The warm pool is generally a bi-product of the cold tongue to the east, which are both created by the climatological Bjerknes feedback. The last finding indicates that the regime behavior depends in essence upon the relative strength of the Bjerknes feedback in the two or more ocean basins. As far as a parameter which can control the relative

feedback strength is systematically varied, one would find the two regimes as in the present study. The split regime can appear only when the Bjerknes feedback works in the two oceans with similar strength and therefore it would be a less dominant state of the Earth's climate.

The above conclusions obtained from coupled models having two different levels of complexity advocate not only that the current climate is strongly constrained by the land configuration but also that we must pay more attention to the coupled feedback between the Indian Ocean and the Pacific in modeling tropical climate and its variability.

Acknowledgments. The author is grateful to Drs. F.-F. Jin and A. Timmerman for stimulating discussion and their constructive comments. Thanks are also due to Drs. J. P. McCreary, S.-P. Xie, N. Schneider, B. Qiu, J.-S. Kug and anonymous reviewers who provided valuable comments. This work was partly supported by a Grant-in-Aid for Scientific Research from MEXT, Japan.

REFERENCES

Anderson, D. L. T., and J. P. McCreary, 1985a: Slowly propagating disturbances in a coupled ocean-atmosphere model. *J. Atmos. Sci.*, **42**, 615-629.

Anderson, D. L. T., and J. P. McCreary, 1985b: On the role of the Indian Ocean in a coupled ocean-atmosphere model of El Nino and the Southern Oscillation. *J. Atmos. Sci.*, **42**, 2439-2442.

Bjerknes, J., 1969: Atmospheric teleconnections from the equatorial Pacific. *Mon. Wea. Rev.*, **97**, 163-172.

Clement, A. C., R. Seager, M. A. Cane, and S. E. Zebiak, 1996: An ocean dynamical thermostat. *J. Climate*, **9**, 2190-2196.

Clement, A. C., R. Seager, and R. Murtugudde, 2005: Why are there tropical warm pools? *J. Climate*, **18**, 5294-5311.

Covey, C., and Co-authors, 2003: An overview of results from the coupled model intercomparison project. *Global Planet. Change*, **37**, 103-133.

Dijkstra, H. A, and J. D. Neelin, 1995: Ocean-atmosphere interaction and the tropical climatology. Part II: Why the Pacific cold tongue is in the east. *J. Climate*, **8**, 1343-1359.

Emori, S., A. Hasegawa, T. Suzuki and K. Dairaku, 2005: Validation, parameterization dependence and future projection of daily precipitation simulated with a high-resolution atmospheric GCM. *Geophys. Res. Lett.*, **32**, doi:10.1029/ 2004GL022306.

Fu, X., B. Wang, D. E. Waliser, and L. Tao, 2007: Impact of atmosphere-ocean coupling on the predictability of monsoon intraseasonal oscillations. *J. Atmos. Sci.*, **64**, 157-174.

Hartmann, D. L., and M. L. Michelsen, 1993: Large-scale effects on the regulation of tropical sea surface temperature. *J. Climate*, **6**, 2049-2062.

Hellerman, S., and M. Rosenstein, 1983: Normal monthly windstress over the world ocean

with error estimates. *J. Phys. Oceanogr.*, **13**, 1093-1104.

Jin, F.-F., 1996: Tropical ocean-atmosphere interaction, the Pacific cold tongue, and the El Niño-Southern Oscillation. *Science*, **274**, 76-78.

Jin, F.-F., 1997: An equatorial ocean recharge paradigm for ENSO. Part I: Conceptual model. *J. Atmos. Sci.*, **54**, 811-829.

Kalnay, E., and Co-authors, 1996: The NCEP/NCAR 40-year reanalysis project. *Bull. Amer. Meteor. Soc.*, **77**, 437-471.

K-1 model developers, 2004: K-1 coupled model (MIROC) description. K-1 Technical Report, **1**, Hasumi, H., and S. Emori (eds.), Center for Climate System Research, University of Tokyo, 34pp.

Kimoto, M., 2005: Simulated change of the East Asian circulation under the global warming. *Geophys. Res. Lett.*, **32**, doi:10.1029/2005GL023383.

Li, T., T. F. Hogan, and C.-P. Chang, 2000: Dynamic and thermodynamic regulation of ocean warming. *J. Atmos. Sci.*, **57**, 3353-3365.

Lin, J.-L., and Coauthors, 2005: Tropical intraseasonal variability in 14 IPCC AR4 climate models Part I: Convective signals. submitted to *J. Climate*, **19**, 2665-2690.

McCreary, J. P., and P. Lu, 1994: Interaction between the subtropical and equatorial ocean circulations: The subtropical cell. *J. Phys. Oceanogr.*, **24**, 466-497.

Neelin, J. D., 1990: A hybrid coupled general circulation model for El Niño studies. *J. Atmos. Sci.*, **47**, 674-693.

Neelin, J. D., and H. A. Dijkstra, 1995: Ocean-atmosphere interaction and the tropical climatology. Part I: The dangers of flux-correction. *J. Climate*, **8**, 1325-1342.

Nozawa, T., T. Nagashima, H. Shiogama, and S. A. Crooks, 2005: Detecting natural influences on surface air temperature change in the early twentieth century. *Geophys. Res. Lett.*, **32**, doi:10.1029/2005GL023540.

Pierrehumbert, R. T., 1995: Thermostats, radiator fins, and the runaway greenhouse. *J. Atmos. Sci.*, **52**, 1784-1806.

Potemra, J. T., and N. Schneider, 2007: Influence of low-frequency Indonesian throughflow transport on temperatures in the Indian Ocean in a coupled model. *J. Climate*, **20**, 1339-1352.

Rayner, N. A., and Coauthors, 2003: Global analyses of sea surface temperature, sea ice, and night marine air temperature since the late nineteenth century. *J. Geophys. Res.*, **108**, doi:10.1029/2002JD002670.

Ramanathan, V., and W. Collins, 1991: Thermodynamic regulation of ocean warming by cirrus clouds deduced from observations of the 1987 El Niño. *Nature*, **351**, 27-32.

Schneider, N., 1998: The Indonesian throughflow and the global climate system. *J. Climate*, **11**, 676-689.

Song, Q., G. A. Vecchi, and A. J. Rosati, 2007: The role of the Indonesian throughflow in the Indo-Pacific climate variability in the GFDL coupled climate model. *J. Climate*, **20**, 2434-2451.

Sun, D.-Z., and Z. Liu, 1996: Dynamic ocean-atmosphere coupling: A thermostat for the tropics. *Science*, **272**, 1148-1150.

Watanabe, M., and F.-F. Jin, 2003: A moist linear baroclinic model: Coupled dynamical-convective response to El Niño. *J. Climate*, **16**, 1121-1139.

Watanabe, M., 2007: Two regimes of the equatorial warm pool. Part I: A simple tropical climate model. *J. Climate*, submitted.

FIGURE CAPTIONS

Fig.1 Observed annual mean climatology of (a) SST and (b) precipitation. The contour intervals are 3 K and 2 mm day^{-1}, respectively. The light (dark) shading indicates values greater than 26 °C (28 °C) in (a) and 4 mm day^{-1} (8 mm day^{-1}) in (b). (c) Standard deviation of observed monthly-mean SST anomalies. The contour interval is 0.1 K while the light (dark) shading indicates values greater than 0.5 K (0.75 K). (d)-(f) As in (a)-(c) but for the climatology obtained from the 100yr control experiment of the HCM.

Fig.2 Annual mean climatology in A0. (a) SST (shading) and the thermocline depth (contour), (b) precipitation, and (c) evaporation (contour) and the surface wind (vector). The contour intervals are 50 m in (a) and 1 mm day^{-1} in (b)-(c). The 26 °C isotherm is indicated by white contour in (a) while the light (dark) shading denotes values greater than 4 mm day^{-1} (8 mm day^{-1}) in (b)-(c). Thick rectangles represent the idealized continents.

Fig.3 Time-longitude section of monthly SST averaged in 10°S-10°N obtained from (a) A0 and (b) A14. The contour interval is 2 K while the light (dark) shading indicates values greater than 24 °C (26 °C).

Fig.4 Scatter plot of SST anomalies between the eastern equatorial Indian Ocean and the Pacific obtained from (a) A0 and (b) A14. Dots are the monthly mean anomalies while circles denote their 13mo running means. A preferred transition route is indicated by grey arrows in (a).

Fig.5 Lagged composites along the equator of (a) SST, (b) thermocline depth (contour) and surface stress (vector), and (c) precipitation (contour) and divergent wind at 200 hPa (vector). All quantities are the 13mo running mean anomalies in A0. The

contour intervals are 1 K, 10 m, and 2 mm day^{-1}, respectively. Shading indicates positive anomalies.

Fig.6 As in Fig. 5 but for composite anomaly maps of (a)-(d) SST (thick contour) and thermocline depth (thin contour) and (e)-(h) precipitation (contour) and 925 hPa wind (vector). The lag in year is indicated at the top of each panel. The contour intervals in (a)-(d) are 1 K and 10 m, respectively, while those in (e)-(h) are 1 mm day^{-1}. Dashed contours indicate negative values, zero contours omitted. Light (dark) shading in (e)-(h) denotes anomalies less than -2 mm day^{-1} (greater than 2 mm day^{-1}).

Fig.7 Annual mean climatology of the equatorial SST in the eastern Pacific as a function of α (dots). Error bars indicate one standard deviation of the monthly mean SST variability. Superimposed by triangles are PDF maxima in monthly SST in each experiment.

Fig.8 Observed annual mean climatology of SLP (thin contour with shading) and ω_{500} (thick contour). The contour interval is 5 hPa and $2x10^{-4}$ hPa s^{-1}, respectively, and the light (dark) shading denotes SLP greater than 1015 (1020) hPa. (b) As in (a) but for climatology in A10. (c) As in (b) but for the thermocline depth (contour with shading) and the surface stress (vector). The contour interval is 30 m and the light (dark) shading denotes the depth shallower (deeper) than 120 m (300 m).

Fig.9 (a) July climatology of precipitation (contour) and the surface wind (vector) in A10. The contour interval is 2 mm day^{-1} and the light (dark) shading indicates values greater than 4 mm day^{-1} (8 mm day^{-1}). The thick grey contour denotes the location where the zonal wind vanishes. (b). As in (a) but for E10. (c) Difference in annual mean SST climatology between A10 and E10 (the latter minus former). The contour interval is 0.3 K.

Fig.10 Monthly mean climatology of the surface zonal wind along the equatorial Indian Ocean in E10. The contour interval is 1 m s^{-1} while the shading denotes westerly anomalies. The dashed lines indicate the zero contour of the zonal wind climatology in A10. (b)-(c) As in (a) but for the HCM control experiment and for the NCEP-NCAR reanalysis.

Fig.11 Annual mean climatology of (a) SST and (b) the standard deviation of monthly SST anomalies in the equatorial Atlantic. The results in A0-A14 are all plotted.

Fig.12 As in Fig. 3 but for the plot extended to the Atlantic. The panel (a) is the same as Fig. 3a while (b) is for AP0 (see text for the experiment).

Fig.13 Annual mean climatology of cloud cover obtained from (a) A0 and (b) A14. The contour interval is 0.1 while the light (dark) shading indicates values greater than 0.8 (0.9).

Fig.14 Annual mean climatology of the longwave (thin solid), shortwave (dashed), and net (thick solid) cloud radiative forcing at surface averaged over 10°S-10°N. The unit is W m^{-2} and black (grey) curves are the results in A0 (A14). Longitudes of continents are indicated at the bottom.

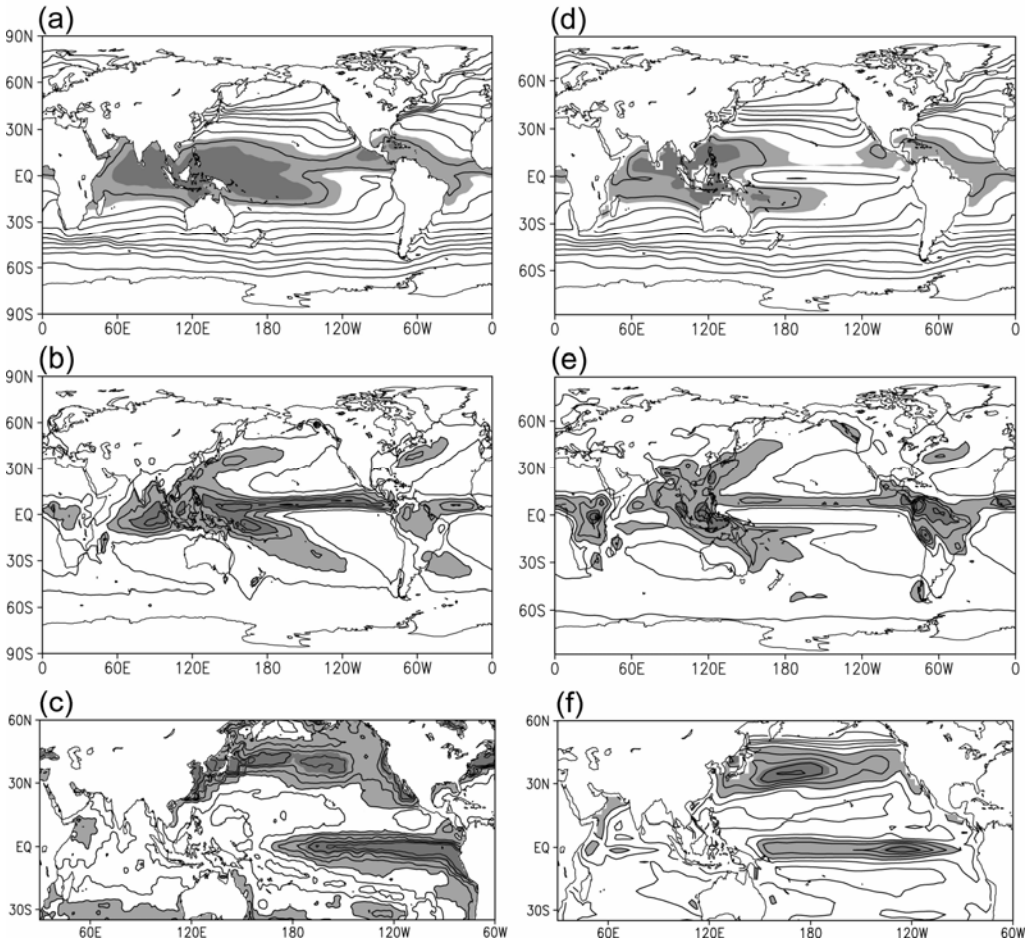

Fig.1 Observed annual mean climatology of (a) SST and (b) precipitation. The contour intervals are 3 K and 2 mm day^{-1}, respectively. The light (dark) shading indicates values greater than 26 °C (28 °C) in (a) and 4 mm day^{-1} (8 mm day^{-1}) in (b). (c) Standard deviation of observed monthly-mean SST anomalies. The contour interval is 0.1 K while the light (dark) shading indicates values greater than 0.5 K (0.75 K). (d)-(f) As in (a)-(c) but for the climatology obtained from the 100yr control experiment of the HCM.

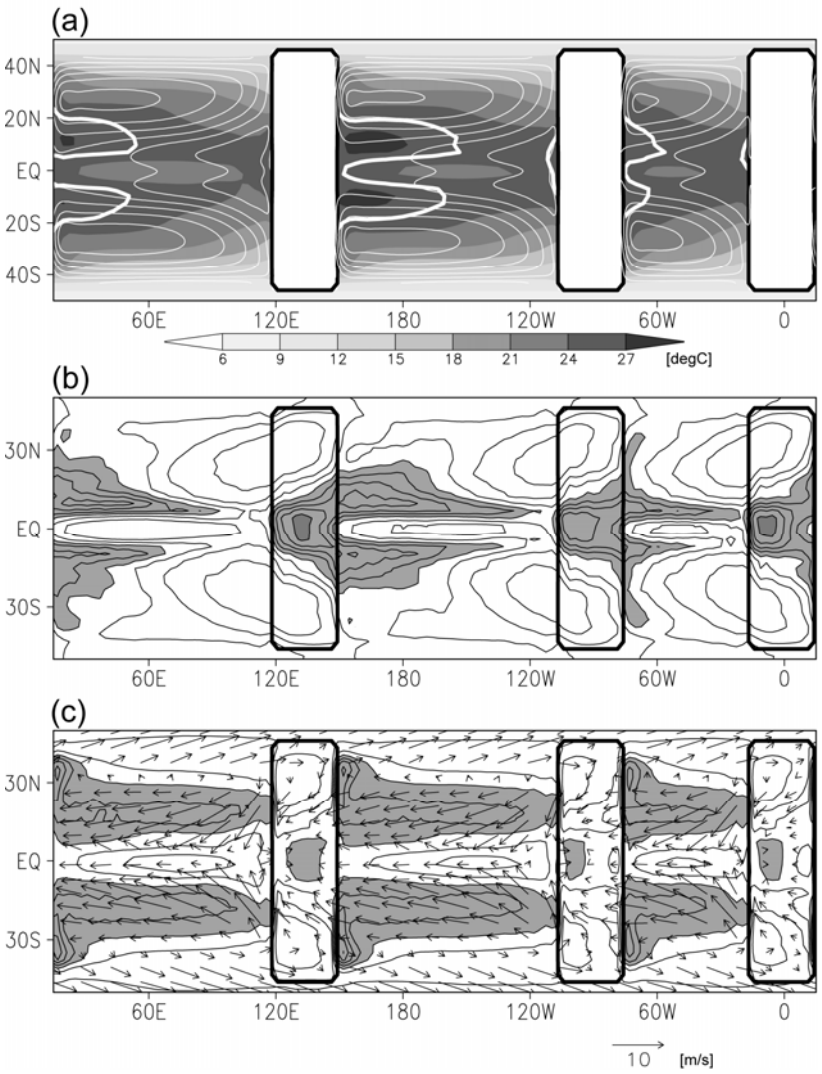

Fig.2 Annual mean climatology in A0. (a) SST (shading) and the thermocline depth (contour), (b) precipitation, and (c) evaporation (contour) and the surface wind (vector). The contour intervals are 50 m in (a) and 1 mm day^{-1} in (b)-(c). The 26 °C isotherm is indicated by white contour in (a) while the light (dark) shading denotes values greater than 4 mm day^{-1} (8 mm day^{-1}) in (b)-(c). Thick rectangles represent the idealized continents.

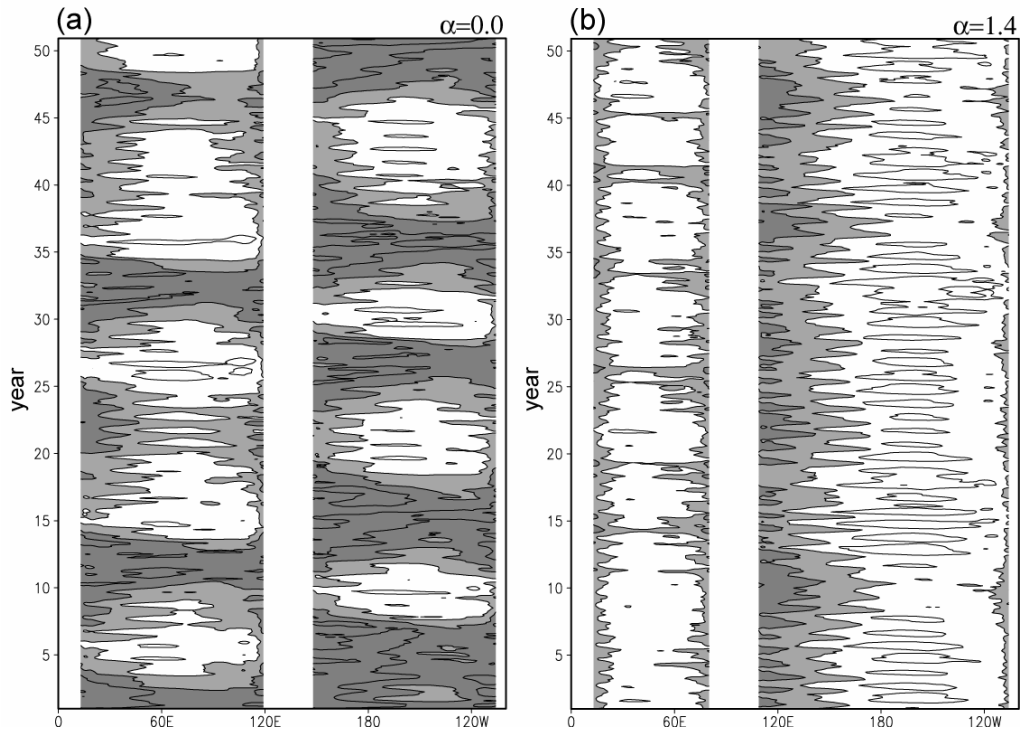

Fig.3 Time-longitude section of monthly SST averaged in 10°S-10°N obtained from (a) A0 and (b) A14. The contour interval is 2 K while the light (dark) shading indicates values greater than 24 °C (26 °C).

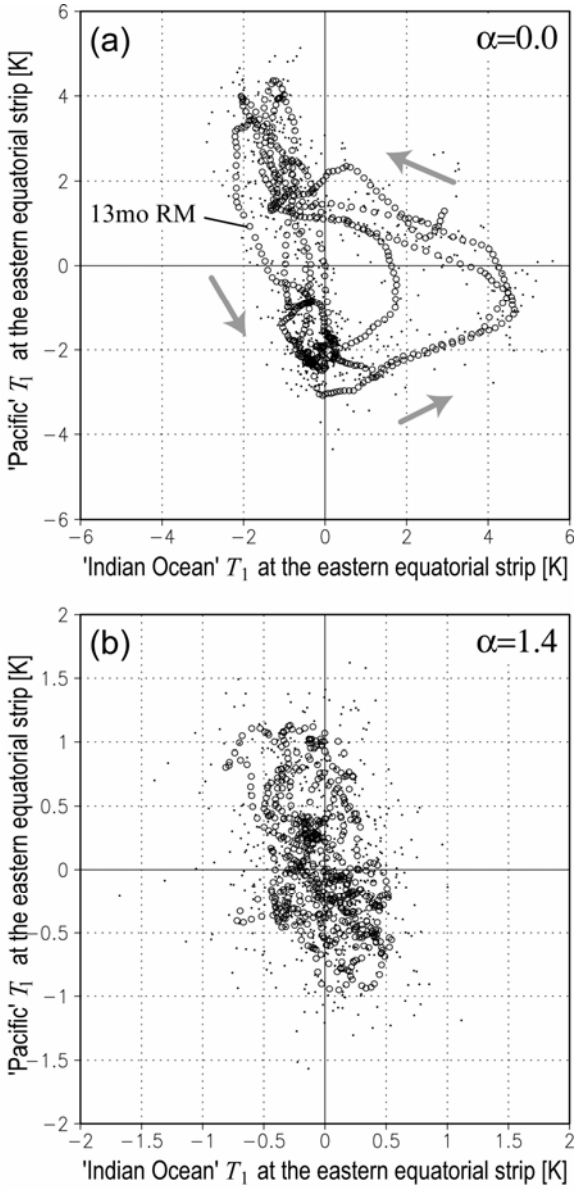

Fig.4 Scatter plot of SST anomalies between the eastern equatorial Indian Ocean and the Pacific obtained from (a) A0 and (b) A14. Dots are the monthly mean anomalies while circles denote their 13mo running means. A preferred transition route is indicated by grey arrows in (a).

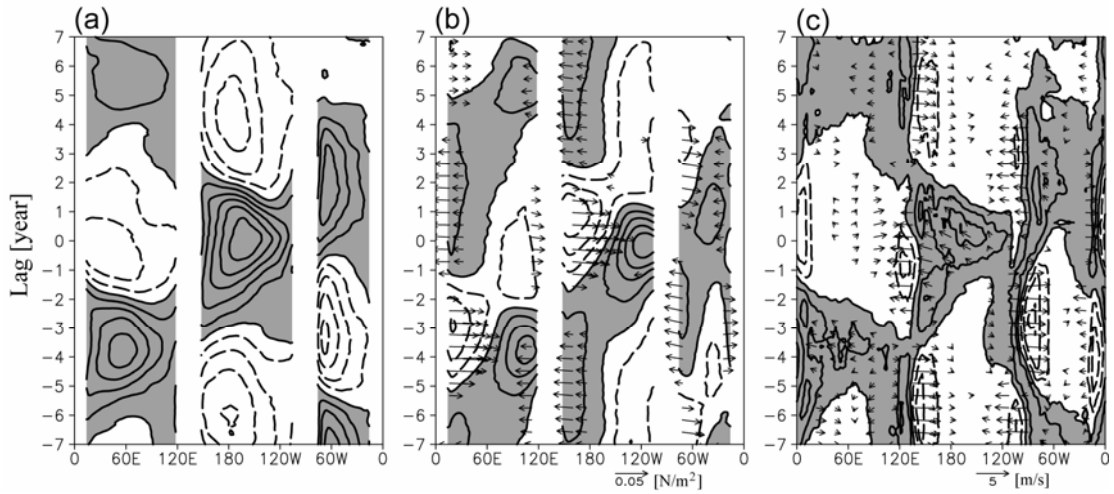

Fig.5 Lagged composites along the equator of (a) SST, (b) thermocline depth (contour) and surface stress (vector), and (c) precipitation (contour) and divergent wind at 200 hPa (vector). All quantities are the 13mo running mean anomalies in A0. The contour intervals are 1 K, 10 m, and 2 mm day^{-1}, respectively. Shading indicates positive anomalies.

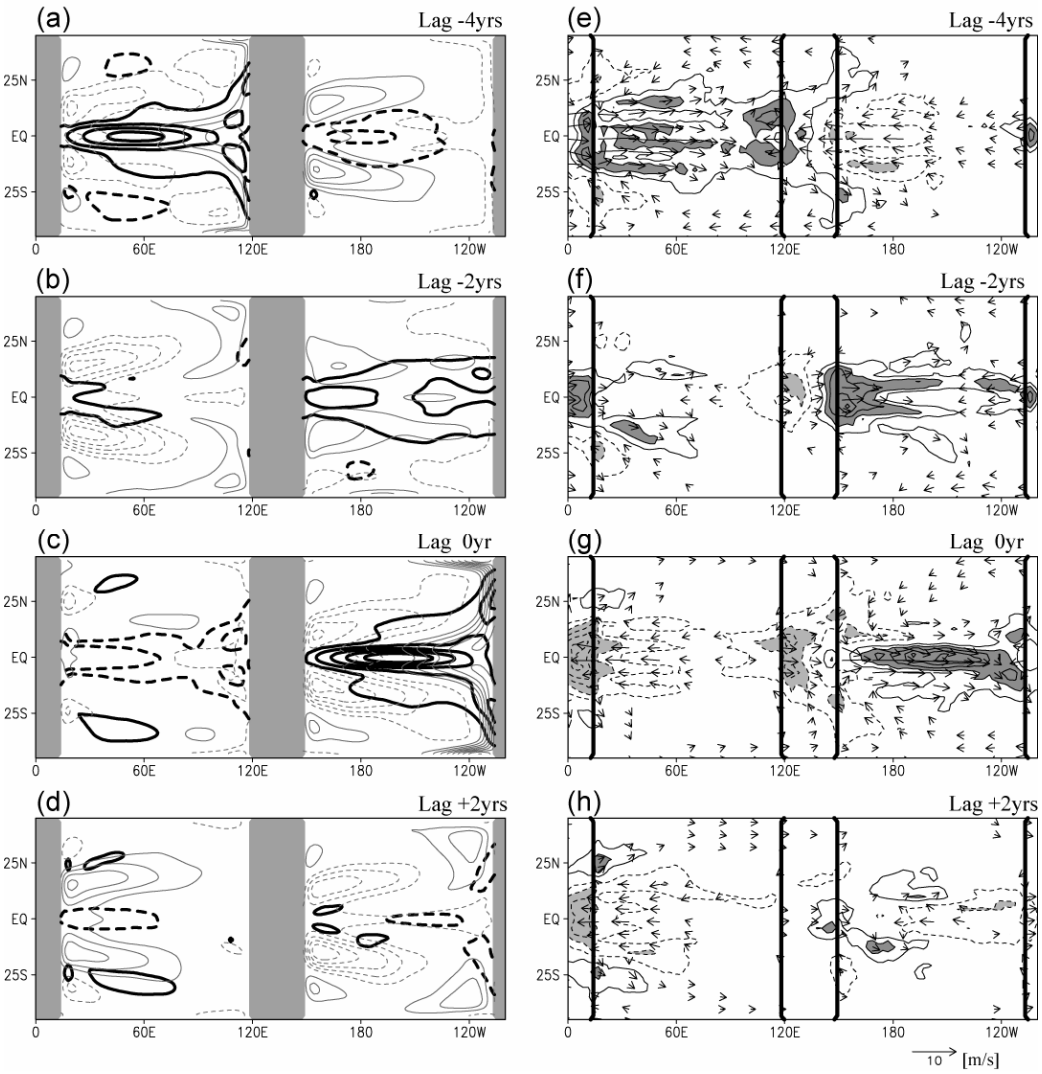

Fig.6 As in Fig. 5 but for composite anomaly maps of (a)-(d) SST (thick contour) and thermocline depth (thin contour) and (e)-(h) precipitation (contour) and 925 hPa wind (vector). The lag in year is indicated at the top of each panel. The contour intervals in (a)-(d) are 1 K and 10 m, respectively, while those in (e)-(h) are 1 mm day^{-1}. Dashed contours indicate negative values, zero contours omitted. Light (dark) shading in (e)-(h) denotes anomalies less than -2 mm day^{-1} (greater than 2 mm day^{-1}).

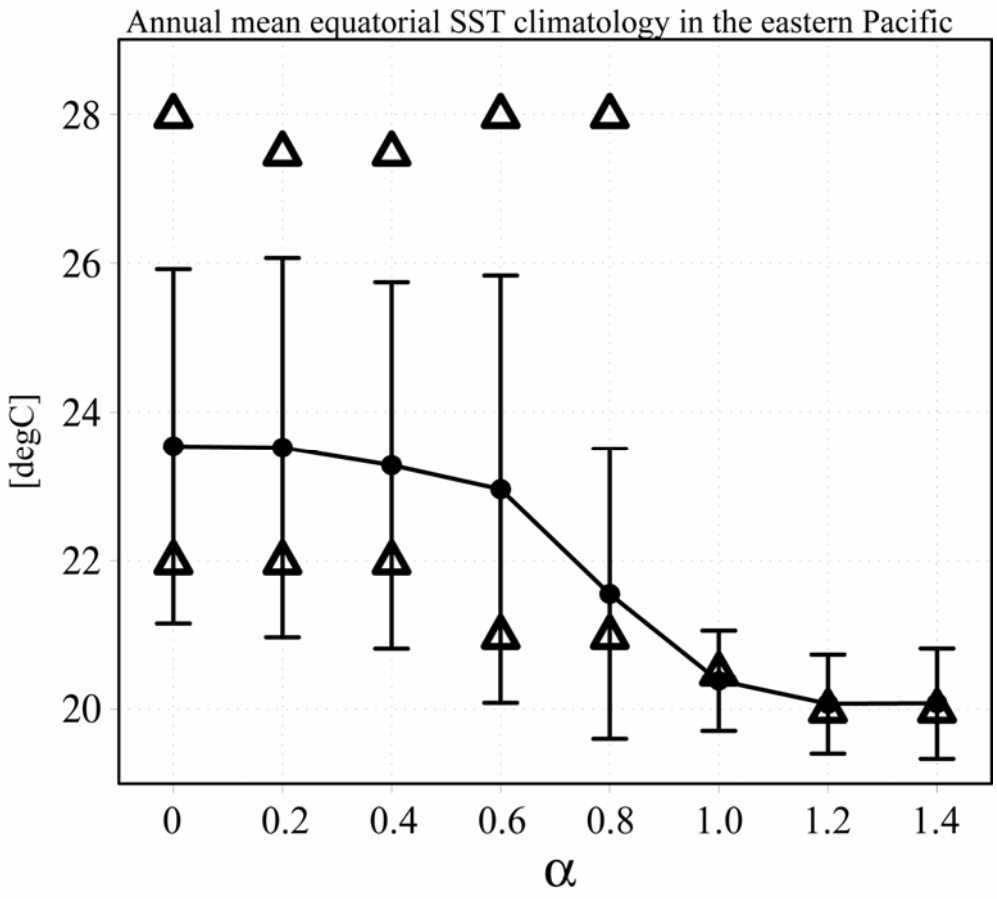

Fig.7 Annual mean climatology of the equatorial SST in the eastern Pacific as a function of α (dots). Error bars indicate one standard deviation of the monthly mean SST variability. Superimposed by triangles are PDF maxima in monthly SST in each experiment.

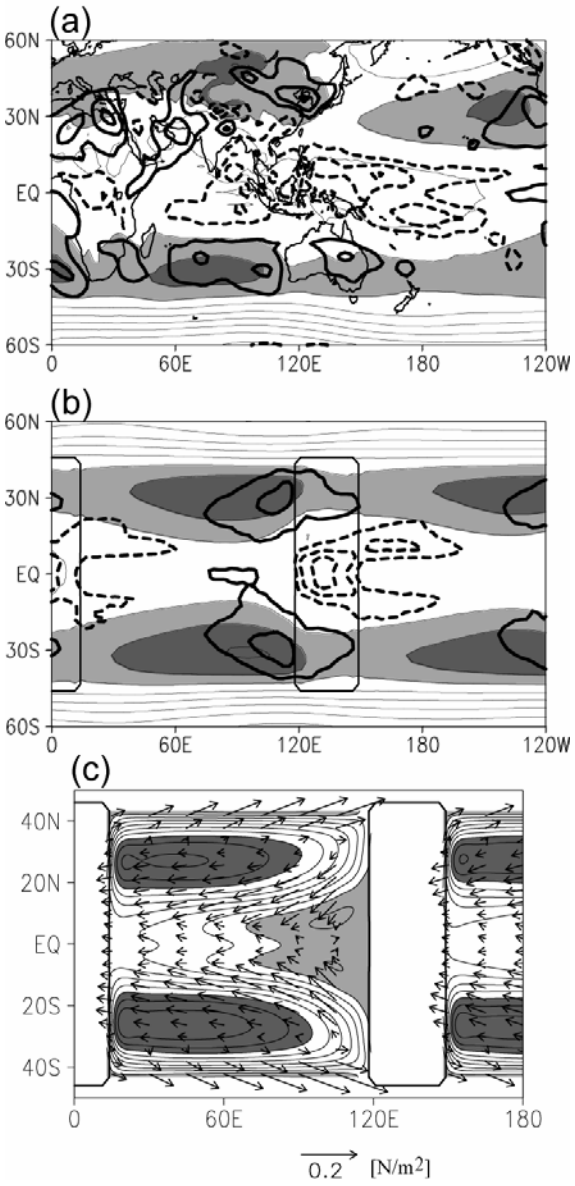

Fig.8 Observed annual mean climatology of SLP (thin contour with shading) and ω_{500} (thick contour). The contour interval is 5 hPa and $2x10^{-4}$ hPa s^{-1}, respectively, and the light (dark) shading denotes SLP greater than 1015 (1020) hPa. (b) As in (a) but for climatology in A10. (c) As in (b) but for the thermocline depth (contour with shading) and the surface stress (vector). The contour interval is 30 m and the light (dark) shading denotes the depth shallower (deeper) than 120 m (300 m).

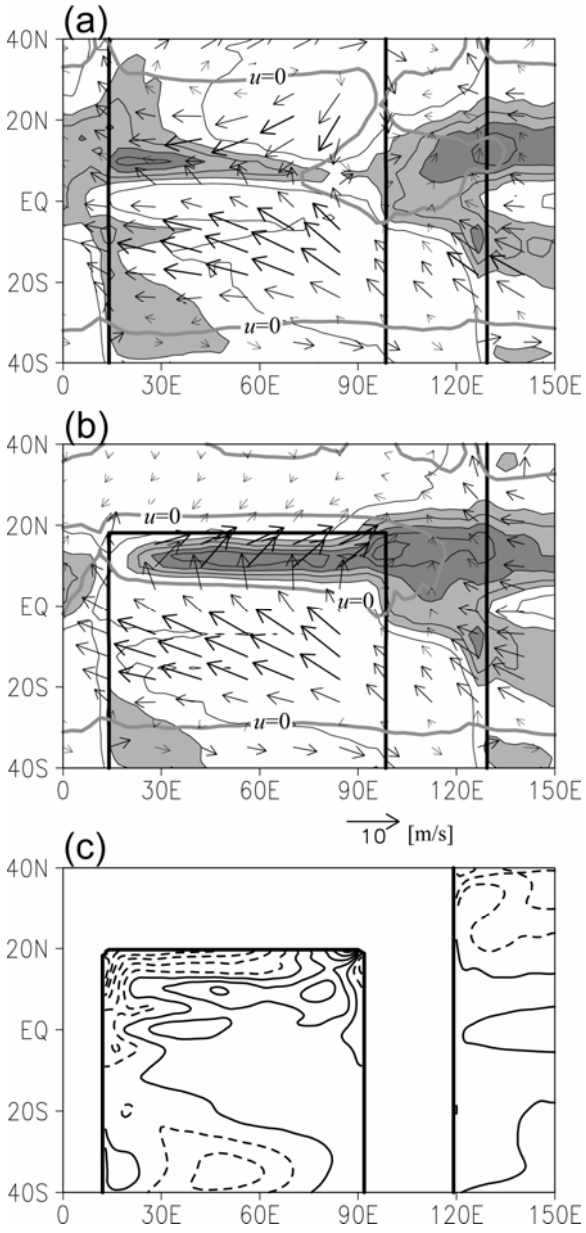

Fig.9 (a) July climatology of precipitation (contour) and the surface wind (vector) in A10. The contour interval is 2 mm day^{-1} and the light (dark) shading indicates values greater than 4 mm day^{-1} (8 mm day^{-1}). The thick grey contour denotes the location where the zonal wind vanishes. (b). As in (a) but for E10. (c) Difference in annual mean SST climatology between A10 and E10 (the latter minus former). The contour interval is 0.3 K.

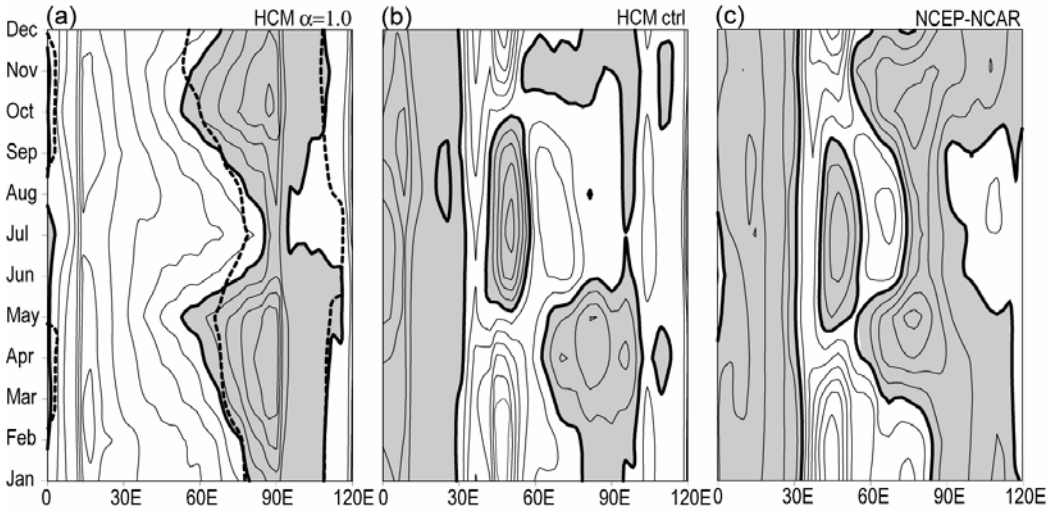

Fig.10 Monthly mean climatology of the surface zonal wind along the equatorial Indian Ocean in E10. The contour interval is 1 m s^{-1} while the shading denotes westerly anomalies. The dashed lines indicate the zero contour of the zonal wind climatology in A10. (b)-(c) As in (a) but for the HCM control experiment and for the NCEP-NCAR reanalysis.

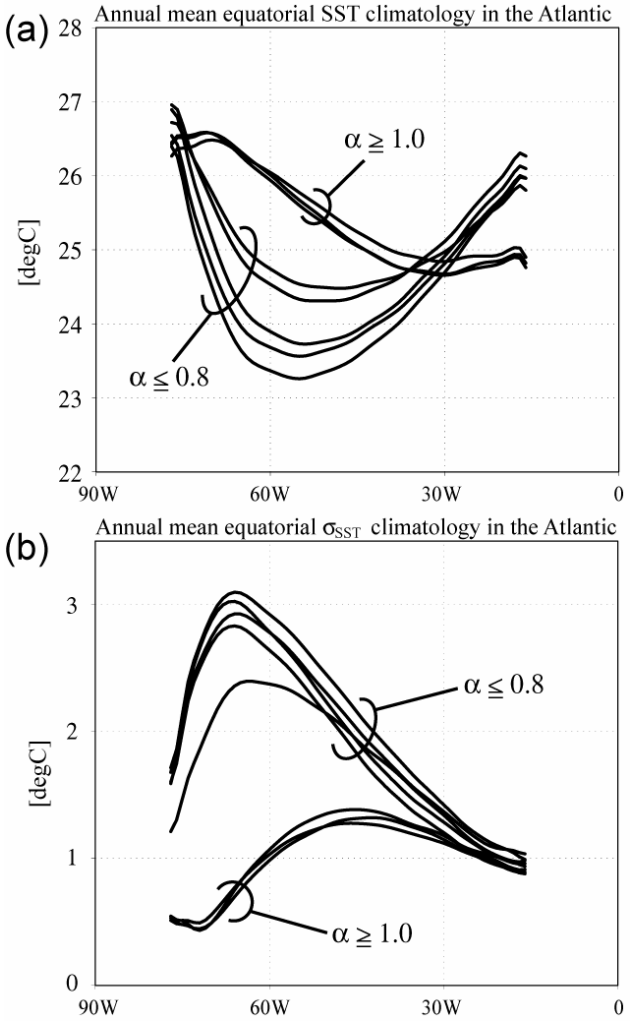

Fig.11 Annual mean climatology of (a) SST and (b) the standard deviation of monthly SST anomalies in the equatorial Atlantic. The results in A0-A14 are all plotted.

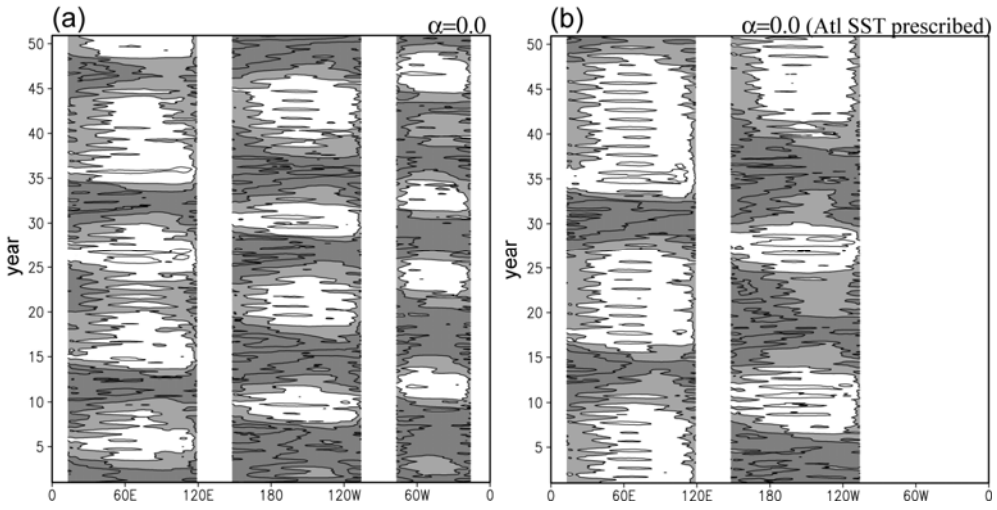

Fig.12 As in Fig. 3 but for the plot extended to the Atlantic. The panel (a) is the same as Fig. 3a while (b) is for AP0 (see text for the experiment).

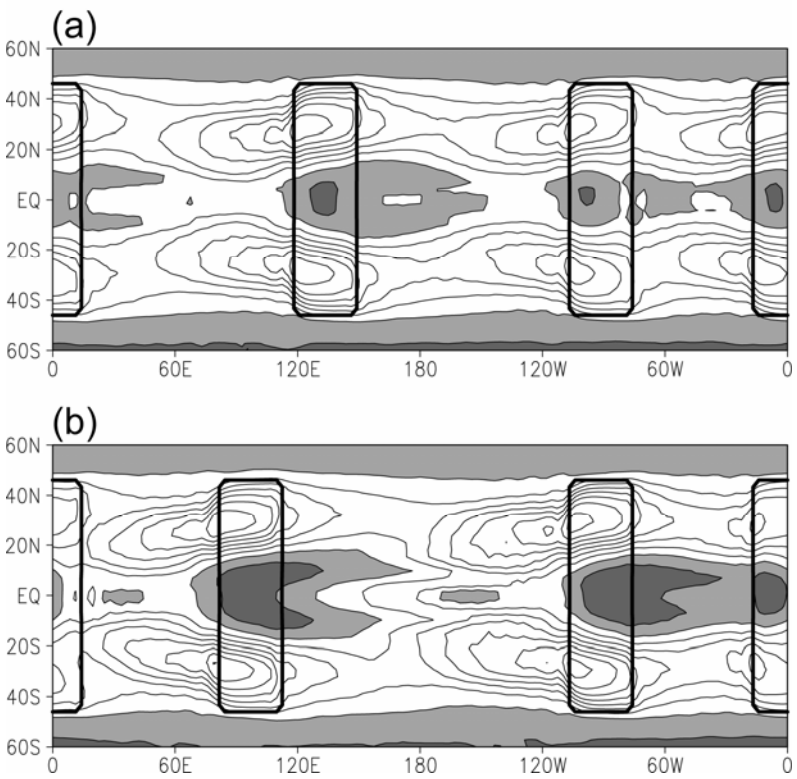

Fig.13 Annual mean climatology of cloud cover obtained from (a) A0 and (b) A14. The contour interval is 0.1 while the light (dark) shading indicates values greater than 0.8 (0.9).

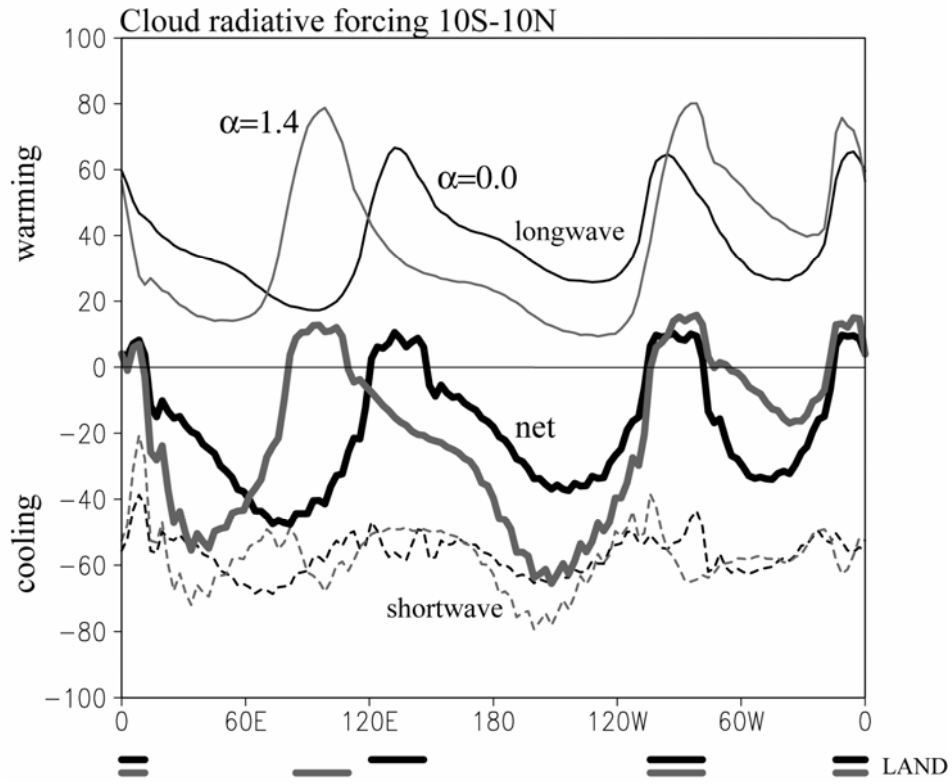

Fig.14 Annual mean climatology of the longwave (thin solid), shortwave (dashed), and net (thick solid) cloud radiative forcing at surface averaged over 10°S-10°N. The unit is W m^{-2} and black (grey) curves are the results in A0 (A14). Longitudes of continents are indicated at the bottom.